

Copyright is owned by the Author of the thesis. Permission is given for a copy to be downloaded by an individual for the purpose of research and private study only. The thesis may not be reproduced elsewhere without the permission of the Author.

Advanced platform for shelf life extension in liquid foods

A thesis presented in partial fulfillment of the requirements for the degree of

Doctor of Philosophy

in

Bioprocess Engineering

At Massey University, Palmerston North

New Zealand

Colin Brown

2012

Summary

The shelf life of lipid based foods is often determined by the development of rancid flavours attributed to lipid oxidation reactions. These reactions are highly complicated and readily change when the reaction system is altered. As a result, researchers have struggled to make significant advances in their understanding of the mechanisms and rates of lipid oxidation.

This thesis focuses on the generalised three step mechanism of lipid oxidation and develops understanding, through mathematical modelling exercises, about the factors that influence the rates of lipid oxidation. More specifically, this thesis focuses on bulk oils, bulk oils with added antioxidants, oil-in-water emulsions and the effects of oxygen supply and consumption rates in real food systems.

For this thesis, methods were developed to identify and validate findings that suggest that lipid hydroperoxides are the rate defining reactant in lipid oxidation reactions. These methods were then used to measure the solubility of oxygen in oil and to define the role oxygen plays in determining the rates of lipid oxidation in a range of systems.

The use of a newly developed batch oxidation apparatus led to the development and validation of models to predict the rates of oxygen consumption during oxidation. The model showed that the rates of oxygen consumption were half order with respect to the lipid hydroperoxide concentration. Through further validation experiments, it was shown that, during the initial stages of lipid oxidation before rancidity, each mole of lipid hydroperoxides formed required 5.04 moles of oxygen to be consumed when there was oxygen present.

The same model and methods were then used to predict the changes in rates of lipid oxidation triggered by changes in reaction temperature. From this work, it was found that the Arrhenius law was capable of predicting the rates of oxygen consumption.

The addition of butylated hydroxyanisole (BHA) to mixed fish oil samples brought with it a reduction in the rates of lipid oxidation, the magnitude of which was proportional to the concentration of BHA added. It was found that the inclusion of a modifier into the half order model was capable of predicting the rates of lipid oxidation when antioxidants were added. Methods to quantify the modifier were supplied for future use.

The dilution of bulk oils by the formation of oil-in-water emulsions was also studied. It was found that the rates of lipid oxidation were proportional to the concentration of

lipids in the emulsion. It was shown that the extent of oxidation during a batch oxidation was inversely proportional to the concentration of lipids in the emulsions as the aqueous phase acted as sump of oxygen for reaction in the oil droplets.

Through modelling and short validation exercises, it was shown that changes to the surface area to volume ratio of oil droplets in emulsions had no effect on the rates of oxygen supply/lipid oxidation and that any effects noted in literature are likely to be the result of other surface active compounds.

Finally, a modelling exercise showed that the rates of oxygen consumption via reaction were likely to be significantly faster than the rates of oxygen supply in unmixed systems in polymer packaging and, to some extent, open to the atmosphere. The diffusion of lipid hydroperoxides was shown to be important in bulk oils stored in polymer packaging as it allowed for a greater proportion of the oil to react with the oxygen transferred, thus reducing the potential for the oxygen supplied to take part in secondary and tertiary product formation. It was suggested that it is better, for a given quantity of oxygen supplied, for the entire oil product to react as it would result in fewer tertiary products being formed than if the oxygen were to be consumed at the surface of the oil only. Following this, it was suggested that an oil-in-water emulsion should be less stable than a bulk oil.

Short experimental work showed that storing bulk oils in the absence of oxygen brings with it a decrease in the rates of lipid oxidation caused by a decrease in the concentration of lipid hydroperoxides. This decrease, coupled with anecdotal evidence that products do become rancid over long periods of time, suggests that the radicals formed during lipid hydroperoxide breakdown can be used in two different sets of reactions. That is, the relative rates of reformation of lipid hydroperoxide via reaction with lipids and the formation of tertiary oxidation products will likely determine the rates of lipid hydroperoxide breakdown and rancidity in real food systems.

An indepth analysis of lipid hydroperoxide breakdown rates in the absence of oxygen as well as a set of validation experiments for the storage of bulk oils and oil-in-water emulsions in polymer films was suggested as being the final piece of information needed to complete a comprehensive model capable of quantitatively predicting the rates of lipid oxidation reactions and the shelf life of lipid oxidation prone foods.

Acknowledgements:

I would like to begin by thanking all the staff at Massey University and Heinz Wattie's who have helped me during my project. There are far too many to list but please know that I am extremely grateful. In particular I would like to thank John Edwards and Ann-Marie Jackson at Massey for their patience and for allowing me to fill their labs with the wonderful aromas of fish oil. I promise that the smell will eventually dissipate. I would also like to thank Clive Bardell for constructing the reaction rigs which formed the basis for the work I conducted.

Many thanks goes to those at Wattie's who supported me with my work and provided me with invaluable insight into the processing industry. In particular I would like to thank Willem van de Veen, Sam Bounds, Margaret Bird and Dr Ian Mackay for their guidance, support and inspiration.

I would also like to thank my Massey supervisors, Prof. John Bronlund, A.Prof Brian Wilkinson and Tom Roberson for their support and for generally putting up with me. I have learnt an awful lot over the past few years and, despite the exhaustion that I am feeling right now, have enjoyed being around and working with you. Mostly I would like to thank you for believing in me when I did not.

My family, Mum, Dad and Adele – thank you for your help and support. I am even thankful for the continual badgering about the thesis (please don't quote me). It was you that helped me through the hard times. Last but certainly not least, I would like to thank Nicola for providing me with a new perspective on life and for just being you.

I was told that I should finish off with something profound or interesting. Unfortunately I am all out of profound. Instead I feel that one more plot in my thesis is needed.

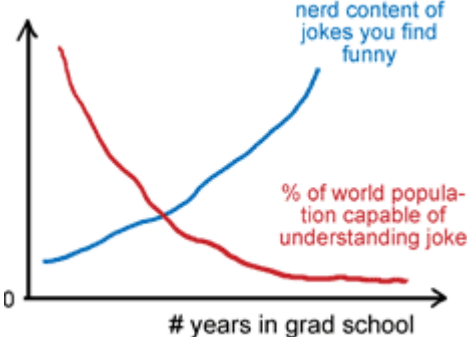


Figure XYZ: Ironically un-funny joke

Table of Contents:

Chapter 1	1
INTRODUCTION	1
1.0 Introduction	2
Chapter 2	7
LITERATURE REVIEW	7
2.0 Introduction	8
2.1 Introduction to lipids and their place in food systems.....	9
Lipid oxidation reactions.....	10
2.1.1 Lipid autoxidation reactions.....	10
2.1.2 Lipid autoxidation initiators.....	12
2.1.3 Free metal ions: catalysis of lipid autoxidation.....	16
2.1.4 Secondary oxidation products by hydroperoxide breakdown..	20
2.2 Antioxidants	22
2.2.1 Primary antioxidants	23
2.2.2 Secondary antioxidants.....	25
2.3 Common methods of detecting & measuring lipid oxidation	26
2.3.1 Peroxide value	27
2.3.2 Para-anisidine value.....	28
2.3.3 Thiobarbiuric acid value	29
2.3.4 Iodine value.....	30
2.3.5 Conjugated dienes.....	31
2.3.6 High performance liquid chromatography.....	32
2.3.7 Gas chromatography	32
2.3.8 Rancimat.....	34
2.3.9 Oxidograph.....	35
2.4 Sensory impact of lipid oxidation.....	36
2.4.1 Sensory and analytical method correlations	37
2.4.2 Partitioning of flavours and its effect on flavour retention	39
2.5 Emulsions	41
2.5.1 Surfactants/emulsifiers.....	41
2.5.2 Main causes of emulsion instability.....	44
2.5.3 Creaming/sedimentation.....	48

2.5.4	<i>Phase inversion</i>	50
2.6	Lipid oxidation in emulsions.....	50
2.6.1	<i>Influence of interfacial region</i>	50
2.6.2	<i>Membrane charge</i>	51
2.6.3	<i>Partitioning of antioxidants</i>	51
2.6.4	<i>pH</i>	53
2.6.5	<i>Droplet size</i>	54
2.7	Packaging and its effects of lipid oxidation reactions.....	55
2.8	Research areas lacking significant investigation to date.....	58
2.8.1	<i>Importance of oxygen as a measure of lipid oxidation</i>	58
2.8.2	<i>Use of oxygen to measure lipid oxidation reaction rates</i>	59
2.8.3	<i>Supply versus consumption of oxygen</i>	61
2.9	Conclusions.....	64
Chapter 3	67
CONCEPTUAL MODEL DEVELOPMENT.....		67
3.0	Introduction.....	68
3.1	Brief description of oxidation system.....	68
3.2	Defining the model required.....	70
3.3	Adding detail to the conceptual model.....	71
3.4	Lipids – investigations on bulk oils.....	71
3.4.1	<i>Reaction mechanism: three stage oxidation pathway</i>	72
3.4.2:	<i>An alternative representation of lipid oxidation</i>	74
3.4.3	<i>Summary hypothesis and mathematical expression</i>	76
3.4.4	<i>Measures of lipid oxidation: pathway and reaction rates</i>	77
3.4.5	<i>Extent of reaction: linking oxygen and lipid hydroperoxides</i> ..	78
3.4.6	<i>Saturation of lipids: stability against oxidation</i>	79
3.4.7	<i>Temperature: reaction rates and the Arrhenius law</i>	80
3.4.8	<i>Antioxidants: delaying lipid oxidation</i>	81
3.4.9	<i>Pro-oxidants: catalysing lipid oxidation</i>	82
3.5	Emulsions – effects of bulk oils in water.....	83
3.5.1	<i>The aqueous phase</i>	84
3.5.2	<i>The interfacial layer</i>	85
3.5.3	<i>Surface area to volume ratio</i>	85

3.6	Oxygen supply and the role of packaging	86
3.6.1	<i>Bulk oils: supply and consumption of oxygen</i>	86
3.6.2	<i>Bulk oils: oxygen supply and consumption rates</i>	87
3.6.3	<i>Diffusion versus reaction in emulsions</i>	89
3.6.4	<i>Diffusion of other reactant species</i>	90
3.7	Conclusions	91
Chapter 4	93
METHOD DEVELOPMENT	93
4.0	Introduction	94
4.1	Lipid oxidation rates.....	94
4.1.1	<i>Measuring lipid oxidation rates</i>	94
4.1.2	<i>Tracking initial versus final products of lipid oxidation</i>	95
4.1.3	<i>Tracking common reactants versus reaction products</i>	96
4.1.4	<i>Method requirements</i>	97
4.2	Design – new method of measuring oxygen consumption.....	98
4.2.1	<i>Rig design: Temperature versus time</i>	98
4.2.2	<i>Rig Design: Homogeneous Reaction</i>	99
4.2.3	<i>Rig design: oxygen supply</i>	99
4.2.4	<i>Rig design: construction</i>	100
4.2.5	<i>Brief operation guide</i>	103
4.3	Dissolved oxygen and fluorescence probe	105
4.3.1	<i>Dissolved oxygen probe operation</i>	105
4.3.2	<i>Probe response to changes in temperature</i>	106
4.3.3	<i>Probe response to changes in media</i>	107
4.4	Rig and method validation.....	109
4.4.1	<i>Oxidation rig – evidence of oxygen exclusion</i>	109
4.4.2	<i>Temperature control</i>	111
4.4.3	<i>Saturation of oil with oxygen</i>	112
4.4.4	<i>Example of dissolved oxygen measurement</i>	115
4.4.5	<i>Repeatability of the oxygen consumption method</i>	116
4.4.6	<i>Effects of half hour sparging on reaction rate</i>	117
4.4.7	<i>Batch oxidation of other oils and oil-in-water emulsions</i>	119
4.5	Conclusion.....	121

Chapter 5	123
BULK OILS - KINETICS.....	123
5.0 Introduction	124
5.1 Empirical models in literature	124
5.2 Mechanistic models in literature	127
5.2.1 <i>The Labuza model</i>	127
5.2.2 <i>The Del Nobile model</i> :.....	131
5.2.3 <i>The Coutelieris and Kanavouras model</i>	135
5.2.4 <i>The Takahashi model</i>	137
5.3 Investigating the Takahashi model – application in a batch system ..	142
5.3.1 <i>Takahashi model – batch oxidation sensitivity analysis</i>	143
5.3.2 <i>Batch oxidation and initial lipid hydroperoxide concentrations</i> ..	148
5.4 Initial oxygen consumption investigations.....	150
5.4.1 <i>Fitting the Labuza model to the initial investigations</i>	151
5.5 Conclusions	152
Chapter 6	155
OXIDATION IN BULK OILS	155
6.0 Introduction	156
6.1 Oxygen solubility in oil.....	156
6.1.1 <i>Literature values for oxygen solubility in oil</i>	157
6.1.2 <i>Measuring the solubility of oxygen in oil</i>	159
6.1.3 <i>Oxygen solubility and temperature</i>	163
6.1.4 <i>Oxygen concentration dependence</i>	165
6.2 Applying the half order model.....	167
6.2.1 <i>Takahashi - lipid hydroperoxides and oxygen consumed</i>	168
6.2.2 <i>Lipid hydroperoxide formation versus oxygen consumption</i> ..	172
6.2.3 <i>Expected errors in analysis</i>	177
6.2.4 <i>Exploring the ratio of oxygen consumed to lipid hydroperoxides formed</i>	180
6.3 Fitting the half order model – further validation.....	186
6.4 Reaction rate and temperature changes	190
6.5 Conclusions	194

Chapter 7	195
ANTIOXIDANTS AND LIPID OXIDATION.....	195
7.0 Introduction	196
7.1 Generalised chemistry of antioxidants in bulk oils.....	196
7.2 Kinetics of antioxidant action	199
7.2.1 <i>Antioxidants – mechanism of action</i>	199
7.2.2 <i>Initiation versus propagation reactions</i>	200
7.3 Initial batch oxidations	203
7.4 Modelling antioxidant activity	204
7.5 Experimentation to validate models developed.....	206
7.6 Modelling antioxidant consumption.....	209
7.7 Conclusions	215
Chapter 8	217
OIL-IN-WATER EMULSIONS	217
8.0 Introduction	218
8.1 The emulsion system	219
8.2 Limiting factors in oxidation in oil-in-water emulsions.....	221
8.3 Modelling reaction and diffusion in oil-in-water emulsions	223
8.3.1 <i>Concentration gradients – an investigation</i>	225
8.4 Analytical model of batch oxidation system	232
8.5 Comparisons and validation against experimental data	240
8.5.1 <i>Dilution of bulk oils in emulsions</i>	240
8.5.2 <i>Droplet surface area to volume ratios</i>	245
8.6 Conclusions	247
Chapter 9	249
RATES OF OXYGEN SUPPLY AND REACTION.....	249
9.0 Introduction	250
9.1 Existing models of coupled reaction and diffusion	250
9.2 Oxygen supply vs. reaction	255
9.2.1 <i>Conceptual model development</i>	256
9.2.2 <i>Analytical solution – initial investigations</i>	257
9.2.3 <i>Packaging – reducing oxygen supply rates</i>	263
9.3 Reactant diffusion –full model analysis:	266

9.3.1	<i>Modelling results – open system</i>	269
9.3.2	<i>Modelling results – polymer packaging</i>	272
9.4	Modelling – relative rates of oxygen supply and consumption	276
9.4.1	<i>Rates of oxygen transfer and consumption</i>	276
9.4.2	<i>Amount of oil being oxidised</i>	279
9.4.3	<i>1D modelling – effects of product surface area to volume ratio..</i>	282
9.4.4	<i>Combining SA/V and oxygen concentration gradients</i>	284
9.5	Emulsions and packaging	286
9.6	Lipid hydroperoxide breakdown	289
9.6.1	<i>Implications of lipid hydroperoxide decrease</i>	294
9.7	Conclusions	297
Chapter 10	299
GENERAL DISCUSSION AND CONCLUSIONS	299
10.0	Introduction	300
10.1	Key outputs from this thesis.....	300
10.1.1	<i>New method of measuring lipid oxidation rates</i>	301
10.1.2	<i>New mechanistic model and application with bulk oils</i>	302
10.1.3	<i>Model and modifier for primary antioxidant addition</i>	302
10.1.4	<i>Model for oil-in-water emulsions</i>	303
10.1.5	<i>Lipid oxidation in systems with low oxygen supply rates</i>	303
10.1.6	<i>Lipid hydroperoxide breakdown – initial investigations</i>	304
10.2	Industrial applications of work so far.....	305
10.2.1	<i>Measuring oxygen consumption rates – a quality control tool ..</i>	305
10.2.2	<i>Process and machinery design and ingredient selection</i>	306
10.2.3	<i>Effectiveness of added antioxidants and other reactants</i>	307
10.2.4	<i>Effects and application in manufacturing and storage</i>	308
10.2.5	<i>Oxidation rate determination – a whole food approach</i>	309
10.3	Conclusions and recommendations	310
REFERENCES	311
APPENDIX	325

List of Figures:

Figure 2.1:	Figure, from Kim et al. (2006), shows the type II photooxidation reaction.	13
Figure 2.2:	Figure from Carlsen et al. (2005). Figure describing Fenton-like oxidation/reduction of heme-iron by peroxides.	18
Figure 2.3:	Figure from Carlsen et al (2005). Figure describes the oxidation of heme- Fe(III) to higher oxidation states.	18
Figure 2.4:	Figure from Carlsen et al. (2005). Figure shows the interaction of three suggested mechanisms of heme-iron catalysed lipid oxidation reactions.	19
Figure 2.5:	Figure shows the two potential breakdown products of lipid hydroperoxides. According to Min & Lee (1999), alkoxy and hydroxyl radical products are preferred.	21
Figure 2.6:	Decomposition of lipid-hydroperoxides to form secondary oxidation products. Figure from Choe & Min (2006).	22
Figure 2.7:	Figure from Huang et al. (1996a). Figure describes the reduction in the rate of lipid hydroperoxide and hexanal production from linoleic acid with different antioxidants added.	24
Figure 2.8:	Figure from Gutierrez & Fernandez (2002). Figure shows the typical peaks formed when PV values are plotted against time.	28
Figure 2.9:	Figure from Osborn & Akoh (2004). Figure shows a typical graph obtained when AV is plotted against time.	29
Figure 2.10:	Figure from Makhoul et al. (2006). Figure shows the correlation between PV and CV for times less than that required to produce a peak concentration of hydroperoxides.	31
Figure 2.11:	Figure from Richards et al. (2005). Figure shows a typical chromatogram in which each peak corresponds to a different compound and concentration. Major peaks include: (7) hexanal, (10) limonene, (19) trans-3,5-octadien-2-one/nonanal	33
Figure 2.12:	Figure from Andersson and Lingnert (1999). Figure shows how GC can be used to track changes of head spaces gases over time.	34

Figure 2.13:	a (left) - from Jacobsen (1999). Relationship between the PV and acceptability for fish oil enriched spreads b (right) - from Jacobsen (1999). Relationship between the AV and acceptability for fish oil enriched spreads	38
Figure 2.14:	Figure taken from Cho et al. (2010). Peroxide values (POV) of olive oil stored in corn zein/soy protein isolate bilayer film pouches (dotted line) and in NY/mLLDPE pouches (solid line) at 50°C. Shape of points represents different storage relative humidities (-O- 30%, -□ 40%, -□ 50%)	58
Figure 3.1:	Depiction of the oxidation system containing oil droplets suspended in an aqueous phase and packaged in a polymer pouch.	68
Figure 3.2:	Revised lipid oxidation pathway including the equilibrium between radical species and lipid hydroperoxides. The thickness of the lines represents the relative amount of each of the reactions that takes place during the development of rancidity in oils	75
Figure 3.3:	Schematic demonstration of the outcomes caused by altering the relative rates of oxygen supply and reaction.	89
Figure 3.4:	Figure depicting the movement of oxygen past oil droplets suspended in an unmixed emulsion.	91
Figure 4.1:	Schematic of the plunger part of the oxidation rig.	101
Figure 4.2:	Schematic of the main reaction chamber and base.	102
Figure 4.3:	Photos of (a) the main reaction vessel, plunger and septum sampling port; (b) A close up of the septum sampling port with a septum installed; (c) The plunger unit	103
Figure 4.4:	Schematic depicting the operation of the oxidation rig and dissolved oxygen probe.	104
Figure 4.5:	Plot showing the effects of temperature on the response from the dissolved oxygen probe. Note that the partial pressure of oxygen in solution was maintained by sparging with air or nitrogen at the given temperature.	107
Figure 4.6:	Results of a storage test to prove the rig's ability to exclude oxygen. Test carried out at 35°C.	110
Figure 4.7:	Temperature in the incubator with a set point of 35°C.	111

Figure 4.8:	Oxygen probe response while in the exit gas stream above a sample of mixed fish oil at 35°C. Initial results are during sparging with nitrogen, followed by sparging with air.	113
Figure 4.9:	Plot to estimate the mass transfer coefficient k_{La} for sparging of mixed fish oil with 0.2 L.min ⁻¹ air at 35 °C	115
Figure 4.10:	Dissolved oxygen profiles for mixed fish oil oxidised (batch) three times at 35 °C	116
Figure 4.11:	Results of three separate batch oxidations of fish oil.	117
Figure 4.12:	Oxygen consumed versus time for three successive batch oxidations a sample of fish oil at 35°C. Note that the plot does not include the time taken for sparging between batch oxidations.	118
Figure 4.13:	Results of batch oxidations of different oils and different temperatures. Temperatures were:	119
Figure 4.14:	Results of batch oxidations of fish oil-in-water emulsions of different oil concentrations stabilised with 5% w/w lecithin.	120
Figure 5.1:	Plot from Shim and Lee (2011). Results of fitting zero order kinetics to the PVs within and after the induction period.	126
Figure 5.2:	A simplified representation of the reaction scheme being modelled.	128
Figure 5.3:	Figure reproduced from Labuza (1971). Figure shows the change in different oxidation products as a function of time and extent of reaction.	130
Figure 5.4:	Relative oxygen consumption rate as a function of oxygen concentration as predicted by the Kanavouras & Coutelieris model.	136
Figure 5.5a&b:	Figure from Takahashi et al. (2000) showing the experimental results taken from the continual oxidation of oleic acid at 333K (triangle), 348K (circle), and 363K (square).	139

- Figure 5.6: Results of applying the Takahashi model at three different temperatures. The solid lines represent the predictions given by the model while the points represent the experimental data (333K - triangle, 348K - circle, and 363K - square). Note that the dotted lines represent a separate model fitted by Takahashi et al. (2000) and have no relevance to this discussion. 140
- Figure 5.7: Figure shows the results of a sensitivity analysis carried out, using the data presented by Takahashi et al. (2000) and reproduced in Tables 5.3 and 5.4. The initial lipid hydroperoxide concentration was set to 0 mol.m⁻³. Note that only the $k_{i2} \cdot 1.5$ and $a \cdot 1.5$ lines differ. All the other lines lie on top of each other. 144
- Figure 5.8: Figure shows the results of a sensitivity analysis carried out, using the data presented by Takahashi et al. (2000) and reproduced in Tables 5.3 and 5.4. The initial lipid hydroperoxide concentration was set to 25 mol.m⁻³. Note that only the $k_{i2} \cdot 1.5$ and $a \cdot 1.5$ lines differ. All the other lines lie on top of each other. 144
- Figure 5.9: Note the full Takahashi model has been modified to model a batch system. The models were run at 333K using the rate constants and other system inputs given by Takahashi et al. (2000). Insert shows the difference in the results of the full and reduced Takahashi model. 147
- Figure 5.10: Figure shows the effect of the initial lipid hydroperoxide concentration on the difference between the rate at the beginning and the end of a batch oxidation. 147
- Figure 5.11: Plot showing the ability of a half order model to fit three successive batch oxidation of mixed fish oil at 40°C. 152
- Figure 6.1: Figure shows the relationship between the temperature and oxygen solubility's for different fish oils. Figure created from data presented by Ke & Ackman (1973). 158
- Figure 6.2: Example plot of the results gained by measuring the partial pressure of oxygen in the air exiting a sample of oil, initially free of oxygen, being sparged with air (atmospheric pressure) at 35°C. 161

Figure 6.3:	Example plot illustrating the difference in results gained by allowing for the time taken for the oxygen probe to respond to changes in oxygen in the oil. Data gained from sparging a sample of oil, initially free of oxygen, with air at atmospheric pressure at 35°C.	162
Figure 6.4:	Change in oxygen solubility with temperature for sample of mixed fish oil (Bakels Ltd, NZ)	164
Figure 6.5:	Results of three successive batch oxidations of a single sample of mixed fish oil at 45°C.	166
Figure 6.6:	Results of a single batch oxidation of flax seed oil at 45°C	167
Figure 6.7:	Results of a simulation of a batch oxidation of oleic acid at 60°C. Model is a modification of the model presented by Takahashi et al. (2000)	169
Figure 6.8:	Results of a simulation of a batch oxidation of oleic acid at 60°C. Model is a modification of the model presented by Takahashi et al. (2000). Insert: Plot of rate of change in lipid hydroperoxide concentration versus the rate of change oxygen concentration.	170
Figure 6.9:	Results of a simulation of a batch oxidation of oleic acid at 60°C. Model is a modification of the model presented by Takahashi et al. (2000).	171
Figure 6.10:	Oxygen consumption profile for samples of mixed fish oil (Bakels Ltd, NZ) at 35°C sparged continuously sparged with air for varying lengths of time.	173
Figure 6.11:	Peroxide values and lipid hydroperoxide concentrations for samples of mixed fish oil (Bakels Ltd, NZ) at 35°C sparged continuously sparged with air for varying lengths of time.	174
Figure 6.12:	Oxygen consumed during sparging of mixed fish oil (Bakels Ltd, NZ) at 35°C	175
Figure 6.13:	Oxygen consumed versus lipid hydroperoxide concentration for continuously sparged mixed fish oil (Bakels Ltd, NZ) at 35°C	176

Figure 6.14:	Resulting oxygen consumed versus lipid hydroperoxide concentration plots for continuously sparged mixed fish oil (Bakels Ltd, NZ) at 35°C when different oxygen solubility values are used. Original solubility: 3.25mol.m ⁻³ . Worst case solubility: 2.82mol.m ⁻³ . One standard error solubility: 3.17mol.m ⁻³ .	177
Figure 6.15:	Plot depicting the errors in PV determination caused by both the end point detection and standardisation of the sodium thiosulphate solution.	178
Figure 6.16:	Plot showing the effects of a 10% error in the PV measured during experimentation.	180
Figure 6.17:	Plot showing the results of individually fitting the half order model to three successive batch oxidations of mixed fish oil (Bakels Ltd, NZ) at 45°C.	182
Figure 6.18:	Plot showing the results of fitting the half order model with a single rate constant (k) to three successive batch oxidations of mixed fish oil (Bakels Ltd, NZ) at 45°C.	184
Figure 6.19:	Plot of results of fitting the half order model with a single rate constant (k) and accounting for the oxygen consumed during sparging and batch oxidation, of three successive batch oxidations of mixed fish oil at 45°C.	185
Figure 6.20:	Plot shows the raw experimental results from batch oxidations of samples of mixed fish oil (Bakels Ltd, NZ) at 35°C sparged for different lengths of time. Smooth lines are the fit produced by fitting the half order model to the raw data.	188
Figure 6.21:	Figure shows the results of experimental and predicted lipid hydroperoxide concentrations for mixed fish oil (Bakels Ltd, NZ) at 35°C that has been sparged with air for different lengths of time.	188
Figure 6.22:	Oxygen consumption profiles for batch oxidations of mixed fish oil (Bakels Ltd, NZ) at different temperatures.	191
Figure 6.23:	Arrhenius plot derived from the data shown in Figure 6.21.	192
Figure 6.24:	Plot shows the Q ₁₀ as a function of time for mixed fish oil (Bakels Ltd, NZ) at reaction temperatures from 35°C to 60°C.	193

Figure 7.1:	The chemical structure of butylated hydroxyanisole (BHA). Figure from Michotte et al. (2011).	197
Figure 7.2:	Possible effect of adding primary antioxidants to bulk oil in a batch oxidation experiment. Action likely if the initiation reactions are a significant source of radical species.	201
Figure 7.3:	Effect of rosemary, cinnamon and clove extracts on the Peroxide Value of hazelnut oil. Figure from Ozcan & Arslan (2011).	202
Figure 7.4:	Effect of Grateloupia Filicina extract and commercial antioxidants on peroxide values of linoleic acid stored at 65°C. Figure from Athukorala et al. (2004).	202
Figure 7.5:	Possible effect of adding primary antioxidants to bulk oil. Action likely if the initiation reactions	203
Figure 7.6:	Results of initial batch oxidations of mixed fish oil samples with and without BHA antioxidant added.	204
Figure 7.7:	Results of batch oxidations of mixed fish oil at 35°C with varying levels of BHA.	206
Figure 7.8:	Example results of fitting the half order model to data obtained from the batch oxidation of mixed fish oil with 500ppm BHA. Figure	207
Figure 7.9:	Results showing the rate constant, k , from batch oxidations of mixed fish oil at 35° with different concentrations of BHA antioxidant.	209
Figure 7.10:	Model results for batch oxidations of mixed fish oil with different concentrations of BHA antioxidant.	211
Figure 7.11:	Model results for batch oxidations of mixed fish oil with different concentrations of BHA antioxidant.	212
Figure 7.12:	Model results for batch oxidations of mixed fish oil with different concentrations of BHA antioxidant.	213
Figure 7.13:	Model results for the continuous oxidation of mixed fish oil with concentrations of BHA antioxidant.	214
Figure 7.14:	Model results for the continuous oxidation of mixed fish oil with different concentrations of BHA antioxidant.	214
Figure 8.1:	Schematic of a spherical droplet of oil surrounded by a sphere of water. Note R_0 is half the centre to centre distance between adjacent oil droplets.	219

- Figure 8.2: Results showing the concentration of oxygen as a function of the distance from the centre of the oil droplet at different time intervals during a batch oxidation of a 20% w/w fish oil in water emulsion. Solid lines represent the droplet surface and outer edge of aqueous phase. 227
- Figure 8.3: Model results showing the difference in oxygen concentration between the centre and surface of the oil droplet during a batch oxidation of 20% w/w mixed fish oil emulsions with different droplet sizes. Note: SA/V for each emulsion is shown in brackets in the key of the plot. 228
- Figure 8.4: Model results showing the amount of oxygen transferred across the droplet surface during a batch oxidation of 20% w/w fish oil-in-water emulsions with different sized droplets (and SA/V's). 229
- Figure 8.5: Model results showing the difference in oxygen concentrations as a function of the distance from the centre of the droplet for 20% w/w fish oil-in-water emulsions made from different droplet sizes. Note: all lines lay on top of one another. Solid lines represent the droplet surface and outer edge of aqueous phase. 231
- Figure 8.6: Results of simulations of oil-in-water emulsions made from the same oil (i.e. with the same reactivity) but with different oil concentrations. 234
- Figure 8.7: Figure shows the relationship between the change in lipid hydroperoxide concentration and oil concentration that can be expected for a single batch oxidation for oil-in-water emulsions. 236
- Figure 8.8: Figure shows the rate of oxygen consumption that can be expected as a function of the lipid hydroperoxide concentration in the oil/emulsion for oil-in-water emulsions containing different concentrations of oils. 237
- Figure 8.9: Figure shows the oxidation continuum for a 20% w/w fish oil-in-water emulsion. That is, the rate of oxygen consumption during a batch oxidation lies on the continuum and its position is described by the initial lipid hydroperoxide concentration. 238

Figure 8.10:	Oxidation continuum for 20% w/w oil-in-water emulsions with initial lipid hydroperoxide concentrations with excess oxygen available.	239
Figure 8.11:	Results of conducting batch oxidation experiments at 45°C on fish oil-in-water emulsions with different oil concentrations. Duplicate of the 5 and 20% emulsions were conducted.	241
Figure 8.12:	Results of batch oxidations at 35°C showing the differences in consumption rates of two oil in water emulsions with different oil concentrations.	242
Figure 8.13:	Figure shows the fit gained by applying the half order model (Equation 8.16) to experimental batch oxidation data for a 5% and a 40% w/w fish oil-in-water emulsions at 35°C.	244
Figure 8.14:	Droplet size distributions of two 20% w/w oil-in-water emulsions (1% lecithin) as measured by the Malvern Mastersizer. The blue line represents an emulsion created by one pass through a Microfluidiser at 690bar while the red line represents the emulsion created by three passes through the Microfluidiser at 1380 bar.	246
Figure 8.15:	Results of batch oxidations of the two 20% w/w fish oil-in-water emulsions with different droplet size distributions (shown in Figure 8.14)	246
Figure 9.1:	Figure from Del Nobile et al. (2003a) showing the model fit to experimental results from long term shelf life experiments of olive oil at 40°C in glass bottles.	254
Figure 9.2:	Figures from Kanavouras & Coutelieris (2005). a) hexanal concentration as a function of time for olive oil stored at 40°C in the dark for olive oil in different packaging materials. b) hexanal concentration as a function of time for olive oil stored at 40°C in light for olive oil in different packaging materials.	254
Figure 9.3:	Figure from Del Nobile et al. (2003a) model predictions and experimental data for the oxidation of olive oil in starch-polymer blend bottles (triangles) and PET bottles (squares) at 40°C.	255

- Figure 9.4: Figure depicting a bulk oil in a polymer package. The package has a length that is many times greater than its width which allows for the assumption that the end effects are negligible. 257
- Figure 9.5: Steady state analysis of oxygen concentration gradients within oil that is open to the atmosphere with potential oil reaction rates. Reaction rates are depicted as the time taken to complete a batch oxidation. 261
- Figure 9.6: Resulting distance from the surface (L) where no oxygen is present as a function of the potential oxygen consumption rate 261
- Figure 9.7: Distance from the surface where oxygen is no longer present (L) as a function of the packaging permeability and the potential rate of oxygen consumption. Note the rate of oxygen consumption is expressed as the time (t) for a batch oxidation. 265
- Figure 9.8: Results from a simulation of a sample of fish oil stored open to the air including the effects of lipid hydroperoxide diffusion. Results show the concentration of lipid hydroperoxides as a function of the distance from the surface of the packaging and for a range of storage times. 269
- Figure 9.9: Results from a simulation of a sample of fish oil stored open to the air including the effects of lipid hydroperoxide diffusion. Results show the concentration of oxygen as a function of the distance from the surface of the packaging and for a range of storage times. 270
- Figure 9.10: Results from a simulation of a sample of fish oil stored open to the air without accounting for lipid hydroperoxide diffusion. Results show the concentration of lipid hydroperoxides as a function of the distance from the surface of the packaging and for a range of storage times. 271
- Figure 9.11: Results from a simulation of a sample of fish oil stored open to the air without accounting for lipid hydroperoxide diffusion. Results show the concentration of oxygen as a function of the distance from the surface of the packaging and for a range of storage times. 272

- Figure 9.12: Results from a simulation of a sample of fish oil stored in 0.25mm thick PET. Results show the concentration of lipid hydroperoxides as a function of the distance from the surface of the packaging and for a range of storage times. 274
- Figure 9.13: Results from a simulation of a sample of fish oil stored in 0.25mm thick PET. Results show the concentration of oxygen as a function of the distance from the surface of the packaging and for a range of storage times. 275
- Figure 9.14: Results of a simulation of fish oil packaged in 0.25mm thick films with different oxygen permeability's. Permeability is presented as a multiple of that for PET (see Table 9.2). 277
- Figure 9.15: Results of a simulation of fish oil packaged in 0.25 mm thick PET. Results show the concentration of lipid hydroperoxides as if the oil were cut into 2mm thick sections beginning at the oil surface. 278
- Figure 9.16: Results of a simulation of fish oil packaged in a 0.25 mm thick with a permeability 20x that of PET. Results show the concentration of lipid hydroperoxides as if the oil were cut into 2 mm thick sections beginning at the oil surface. 279
- Figure 9.17: Results of a simulation of fish oil packaged in 0.25 mm thick PET. Results show the proportion of the total lipid hydroperoxide formed in 2mm thick sections beginning at the oil surface. 280
- Figure 9.18: Results of a simulation of canola oil packaged in a 0.25 mm thick film that has permeability 100x that of PET. Results show the oxygen concentration as a function of time for a range of distances from the surface of the oil. 281
- Figure 9.19: Results of a simulation of canola oil packaged in a 0.25mm thick film that has permeability 100x that of PET. Results show the lipid hydroperoxide concentration as a function of time for a range of distances from the surface of the oil. 282

- Figure 9.20: Rate of oxygen supplied through packaging for a 500 mL sample of oil in a cylindrical package. The oxygen permeance was $4.5 \times 10^{-18} \text{ mol.m}^{-2}\text{Pa}^{-1}\text{s}^{-1}$. 283
- Figure 9.21: Relationship between the surface area and surface area to volume ratio with radius for a cylindrical product with a volume of 500 mL. 284
- Figure 9.22: Proportion of oil with oxygen present as a function of the SA/V for a 500 mL sample of oil in a cylindrical package. The oxygen permeance was $4.5 \times 10^{-18} \text{ mol.m}^{-2}\text{Pa}^{-1}\text{s}^{-1}$ (23°C, 50%RH). End effects were included. 285
- Figure 9.23: Figure shows the effective rate constant for a fish oil-in-water emulsion as a function of the mass fraction of oil in the emulsion. 287
- Figure 9.24: Figure showing the oxygen concentration as a function of time and position for a simulation of a 10% w/w canola oil-in-water emulsion packaged in PP. 288
- Figure 9.25: Figure shows the relationship between the lipid hydroperoxide formed per unit of oil and the concentration of oil in the emulsion. 289
- Figure 9.26: Figure depicts the reactions that compete for the radicals formed from the breakdown of lipid hydroperoxides. 291
- Figure 9.27: Results of batch oxidations of fish oil stored at 37°C in the absence of oxygen. 293
- Figure 9.28: Results comparing the batch oxidation curves of oil stored at 37°C for 28 days and a control oil before storage. 294
- Figure 9.29 a&b: Results gained from work by Alamed et al. (2009) shown the evolution of hexanal and the formation of lipid hydroperoxides from corn oil-in-water emulsions. 296

List of tables:

Table 2.1:	Table from van Ruth et al. (2002). Table shows the partitioning coefficient (x1000) for 20 common volatile products in the oil and water phases of a 20% w/w sunflower in water made with and without Tween emulsifier.	46
Table 2.2:	Permeability data for different polymer packaging materials as given in Frankel (2005); data gained from experiments at 23°C and 50% relative humidity.	57
Table 4.1:	Probe response in different media saturated with 21% oxygen (from air).	108
Table 5.1:	Rate constants developed for the Del Nobile model.	133
Table 5.2:	Rates of lipid hydroperoxide formation and decomposition for different combinations of oxygen and lipid hydroperoxide concentrations as predicted by the Del Nobile model	135
Table 5.3:	Arrhenius constants and activation energies used to estimate the rate constants required in the Takahashi model. Values are taken from Takahashi et al. (2000). These represent model inputs that were used to derive the predictions shown in Figure 5.6.	140
Table 5.4:	Table showing the different mass transport coefficients and saturated oxygen concentrations at the three temperatures used by Takahashi et al. (2000).	141
Table 5.5:	Results gained from a sensitivity analysis concentrating on the remaining terms in Equation 5.42. Note that the value for kI2 was taken directly from Takahashi et al. (2000) for a temperature of 333K.	146
Table 6.1:	Oxygen solubilities in literature for a range of oils. The data presented has been manipulated in order to present them in the same units. Superscripts describe sources of information: a Takahashi et al. (2000), b Lango et al. (1996), c Ke & Ackman (1973), d Del Nobile et al.(2003).	157

Table 6.2:	Calculated oxygen solubilities from replicate experiments using mixed fish oil at 35°C before and after accounting for the response time of the oxygen probe.	163
Table 6.3:	Oxygen solubility in mixed fish oil (Bakels Ltd, NZ) at different temperatures	164
Table 6.4:	Results of individually fitting the half order model to three successive batch oxidations of mixed fish oil (Bakels Ltd, NZ) at 45°C.	183
Table 6.5:	Results of fitting the half order model with a single rate constant (k) to three successive batch oxidations of mixed fish oil at 45°C.	184
Table 6.6:	Results of fitting the half order model with a single rate constant, k, and accounting for the oxygen consumed during sparging and batch oxidation, of three successive batch oxidations of mixed fish oil at 45°C.	186
Table 6.7:	Comparison between measured and predicted lipid hydroperoxide concentrations for mixed fish oil (Bakels Ltd, NZ) at 35°C that has been sparged with air for different lengths of time.	189
Table 7.1:	The rate constants resulting from fitting the half order model to batch oxidations of oil with different concentrations of BHA antioxidant	208
Table 8.1:	Model results showing the change in lipid hydroperoxide concentration that can be expected after a batch oxidation of a fish oil-in-water emulsions containing different concentrations of fish oil.	235
Table 8.2:	Results of measuring the initial and final oxygen consumption rates from data shown in Figure 8.13 as well as the calculated initial lipid hydroperoxide concentrations.	244
Table 9.1:	Results showing the mass transfer coefficient and distance at which no oxygen is present, L, for different air velocities	261
Table 9.2:	Permeability data for different polymer packaging materials as given in Frankel (2005) and converted to SI units. Data gained from experiments at 23°C and 50% relative humidity.	264